A SYMPLECTIC PARTITIONED RUNGE-KUTTA METHOD USING THE EIGHTH-ORDER NAD OPERATOR FOR SOLVING THE 2D ELASTIC WAVE EQUATION

CHAOYUAN ZHANG[1] and LI CHEN[2]

[1] *College of Mathematics and computer, Dali University, Dali 671003, P.R. China.*
zcy_km@163.com
[2] *College of Engineering, Dali University, Dali 671003, P.R. China.*

ABSTRACT

Zhang, C. and Chen, L., 2015. A symplectic partitioned Runge-Kutta method using the eighth-order NAD operator for solving the 2D elastic wave equation. *Journal of Seismic Exploration*, 24: 205-230.

In this paper, on the basis of the extended Hamiltonian system, we develop a symplectic partitioned Runge-Kutta method based on the nearly analytic discrete (NAD) operator with eighth-order accuracy for solving the 2D elastic wave equation, which is called the eighth-order NAD-SPRK method in brief. In the new method, we first employ the NAD operators with the eighth-order accuracy to discretize the high-order partial derivatives of space directions in the 2D elastic wave equation. Then the symplectic partitioned Runge-Kutta scheme with the second-order accuracy is applied to discretize the temporal high-order partial derivatives. We provide the theoretical study on the properties of the eighth-order NAD-SPRK method, such as theoretical error, stability criteria, numerical dispersion, and computational efficiency. We also compare the 2D elastic wave modeling results of this new method against those of some high-order methods. Numerical experiments show that the eighth-order NAD-SPRK method has the least numerical dispersion against the fourth-order NSPRK method, the eighth-order Lax-Wendroff correction (LWC) method, and the eighth-order staggered-grid (SG) method. Meanwhile, its computational costs and memory requirements are much less than those of the eighth-order LWC method. Against the eighth-order LWC method, comparison results indicate that the eighth-order NAD-SPRK method can provide the equivalent solutions with analytic solutions on much coarser grids. Last, we present the wave-field snapshots and wave seismograms in the homogeneous transversely isotropic medium and in the three-layer medium with a fluctuating interface for the 2D elastic wave, and the wave-field snapshots of the 2D elastic wave in the two-layer homogenous isotropic medium and in the two-layer heterogeneous medium. All these results of numerical simulations illustrate that the eighth-order NAD-SPRK method can effectively suppress the numerical dispersion caused by discretizing the wave equations when big grids are used or when models have large velocity contrasts between adjacent layers, further resulting in both saving the storage space and increasing the computational efficiency when too few sampling points per minimum wavelength are used.

KEY WORDS: NAD operator, symplectic partitioned Runge-Kutta method, elastic wave equation, numerical dispersion, wave-field simulation.

INTRODUCTION

Using the inversion imaging method of seismic to know the internal structure of the earth and explore oil resources, requires fast and accurate simulation for the forward process of seismic wave propagating in the earth medium. Therefore, for a long time, to develop a more effective and more accurate forward numerical simulation method has been one of the important research topic in geophysics.

To improve the calculational efficiency and computational accuracy of wavefield simulation in the complex media, many numerical methods since 20 century have been proposed. Currently, the mainly used schemes include finite element methods (Chen, 1984; Ma and Liu, 2006; Moczo et al., 2007; Smith,1975; Yang, 2002), finite difference (FD) schemes (Dablain, 1986; Dong et al., 2000; Kelly et al., 1976; Moczo et al., 2000, 2002; Sänger et al., 2000), pseudo spectral methods (Huang, 1992; Komatitsch and Vilotte, 1998), reflectivity method (Chen, 1993) and so on. Among these numerical techniques, FD methods (Dablain, 1986; Kelly et al., 1976) have become the most used method of wavefield simulation in geophysics because of its simplicity for computer code, fast calculation speed and high parallelism. However, the conventional FD schemes suffer from serious numerical dispersion when too coarse computation grids are used or when the velocity models have strong velocity contrasts between adjacent layers (Dablain, 1986; Yang et al., 2002, 2006, 2012). To suppress numerical dispersion, fine space grids or high-order methods are used usually. Unfortunately, finer grid spacing leads to significant increase in memory usage and computation time of central processing unit. Higher order methods, which are less efficient in the parallel implementation of algorithms and boundary treatments, will not guarantee a necessarily lower phase velocity error of the wave (Fei and Larner, 1995). To effectively solve these existing problems, the so-called nearly analytic discrete (NAD) (Yang et al., 2003) operator was introduced to approximate the partial differential operators based on the truncated Taylor expansion and the local interpolation compensation for the truncated Taylor series. From the NAD operator, different more effective numerical algorithms (Chen et al., 2010; Wang et al., 2009; Yang et al., 2007, 2009) have been developed, which can enable the effective suppression of the numerical dispersion when coarse computation grids are used. However, These methods did not consider the symplectic property of differential operators in the 2D elastic wave equation. At the same time, the NAD operator has only the fourth-order space accuracy, and there is no research on the NAD operator with higher space accuracy at present.

As we know, the Hamiltonian framework possesses elegant symmetric structures inducing several conservation laws such as conservation of symplecticity and energy (Ruth, 1983). It is therefore very important to conserve

numerically these structures for designing numerical schemes to solve Hamiltonian systems that they preserve the physical properties of a system and the numerical stability. For solving seismic wave propagating equations evaluated in the Hamiltonian systems, in the past two decades, many schemes have been proposed and have obtained favourable results (Yoshida, 1993), among which are a number of algorithms that numerically solve the Hamiltonian partial differential equation (PDE). The conventional construction of numerical schemes for the Hamiltonian PDE is to first discretize the spatial derivatives by the second- or fourth-order central-difference schemes to transform the PDEs into a semi-discrete Hamiltonian system of ordinary differential equations, which will then be solved using one of the symplecticity conserving methods (Qin and Zhang, 1990). Recently, a nearly analytic symplectically partitioned Runge-Kutta (NSPRK) method with fourth-order space accuracy has been developed to solve the wave equations (Ma et al., 2011, 2010) and has achieved good results. But the fourth-order NSPRK method has the only fourth-order accuracy in space.

In this paper, on the basis of the extended Hamiltonian system, we propose a symplectic partitioned Runge-Kutta method using NAD operators with eighth-order accuracy for solving 2D elastic wave equations to further reduce the numerical dispersion and further improve the accuracy of the wave-field simulation, which is called the eighth-order NAD-SPRK method in brief. We first transform the original elastic wave equations into a conventional Hamiltonian system. Then, we employ the NAD operators with the eighth-order accuracy (Tong et al., 2013; Zhang et al., 2014a, 2014b) to discretize the high-order partial derivatives of space directions, and apply the symplectic partitioned Runge-Kutta scheme with the second-order accuracy (Sun, 1997) to discretize the temporal high-order partial derivatives. Due to using the symplectic method in time and choosing the high-order NAD operators in space, so the eighth-order NAD-SPRK method has advantages of conserving the symplecticity in time and effectively suppressing the numerical dispersion.

To illustrate the numerical behaviors of this new method, we analyze its theoretical error and stability criteria. We also numerically investigate numerical dispersion, computational efficiency, and numerical solutions. Last, we simulate the elastic wave propagating in the homogeneous transversely isotropic medium, the two-layer homogenous isotropic medium, the two-layer heterogeneous medium, and the three-layer medium with a fluctuating interface. The results of numerical simulations demonstrate that the eighth-order NAD-SPRK method has very low numerical dispersion when coarse grids are used or models have strong velocity contrasts between adjacent layers. As a result, the eighth-order NAD-SPRK method can save both the storage space and computational time when too few sampling points per minimum wavelength are used.

THEORY OF THE EIGHTH-ORDER NAD-SPRK METHOD

Second-order symplectic partitioned Runge-Kutta scheme

Consider the following Hamiltonian system for 2D case

$$
\begin{cases}
dU/dt = V \\
dV/dt = LU
\end{cases}
\qquad , \tag{1}
$$

where $U = (u_1, u_2, u_3)^T$, $V = (v_1, v_2, v_3)^T$, and L is the second-order partial differential operator.

We can discretize the second-order temporal derivatives included in system (1) by using the following second-order symplectic partitioned Runge-Kutta scheme, namely, the Lobatto IIIA-IIIB method (Sun, 1997), to approximate the time derivatives

$$
\begin{cases}
V_1 = V^n + \tfrac{1}{2}\Delta t L U^n \\
U^{n+1} = U^n + \Delta t V_1 \\
V^{n+1} = V_1 + \tfrac{1}{2}\Delta t L U^{(n+1)}
\end{cases}
\qquad , \tag{2}
$$

where Δt is the time step, V_1 is the intermediate variable.

To save storage space and improve calculation speed, by combining with eq. (2), we gain the computational formulae as follow

$$
\begin{cases}
U^{n+1} = V^n + \Delta t V^n + \tfrac{1}{2}\Delta t^2 L U^n \\
V^{n+1} = V^n + \Delta t L U^n + \tfrac{1}{2}\Delta t^2 L V^n + \tfrac{1}{4}\Delta t^3 L^2 U^n
\end{cases}
\qquad , \tag{3}
$$

where $L^2 = L \cdot L$.

Transforms of the elastic wave equations

In 2D inhomogeneous anisotropic medium, the elastic wave equations are given by

$$
\rho(\partial^2 u_i / \partial t^2) = (\partial \sigma_{ij} / \partial x_j) + f_i \ , \quad i = 1,2,3 \tag{4}
$$

where the subscript j takes the values of 1 and 3, u_i and f_i denote the displacement and the force source component in the i-th direction, $\rho = \rho(x,z)$

and σ_{ij} are the density and stress tensor, respectively.

By using the stress-strain relations, we can transform eq. (4) into the following vector equation

$$\partial^2 U/\partial t^2 = DU + F \ , \tag{5}$$

where $U = (u_1, u_2, u_3)^T$, $F = [(1/\rho)f_1, (1/\rho)f_2, (1/\rho)f_3]^T$ and D is the second-order partial differential operator. For examples, for the 2D homogenous isotropic case D_1 is defined by

$$D_1 = \begin{pmatrix} \dfrac{\lambda+2\mu}{\rho}\dfrac{\partial^2}{\partial x^2} + \dfrac{\mu}{\rho}\dfrac{\partial^2}{\partial z^2} & 0 & \dfrac{\lambda+\mu}{\rho}\dfrac{\partial^2}{\partial x\partial z} \\[3mm] 0 & \dfrac{\mu}{\rho}\left(\dfrac{\partial^2}{\partial x^2} + \dfrac{\partial^2}{\partial z^2}\right) & 0 \\[3mm] \dfrac{\lambda+\mu}{\rho}\dfrac{\partial^2}{\partial x\partial z} & 0 & \dfrac{\mu}{\rho}\dfrac{\partial^2}{\partial x^2} + \dfrac{\lambda+2\mu}{\rho}\dfrac{\partial^2}{\partial z^2} \end{pmatrix},$$

and for the 2D transverse isotropic case D_2 is defined by

$$D_2 = \begin{pmatrix} \dfrac{c_{11}}{\rho}\dfrac{\partial^2}{\partial x^2} + \dfrac{c_{44}}{\rho}\dfrac{\partial^2}{\partial z^2} & 0 & \dfrac{c_{13}+c_{44}}{\rho}\dfrac{\partial^2}{\partial x\partial z} \\[3mm] 0 & \dfrac{c_{66}}{\rho}\dfrac{\partial^2}{\partial x^2} + \dfrac{c_{44}}{\rho}\dfrac{\partial^2}{\partial z^2} & 0 \\[3mm] \dfrac{c_{13}+c_{44}}{\rho}\dfrac{\partial^2}{\partial x\partial z} & 0 & \dfrac{c_{44}}{\rho}\dfrac{\partial^2}{\partial x^2} + \dfrac{c_{33}}{\rho}\dfrac{\partial^2}{\partial z^2} \end{pmatrix},$$

where λ, μ, c_{ij} are the elastic constants.

Let $v_i = \partial u_i/\partial t$ $(i = 1,2,3)$ and $V = (v_1, v_2, v_3)^T$. Then eq. (5) can be rewritten as

$$\begin{cases} \partial U/\partial t = V \\ \partial V/\partial t = DU + F \end{cases} . \tag{6}$$

After we define the notations of $\bar{U} = (U, \partial U/\partial x, \partial U/\partial z)^T$, $\bar{V} = (V, \partial V/\partial x, \partial V/\partial z)^T$ and $\bar{F} = (F, \partial F/\partial x, \partial F/\partial z)^T$, eq. (6) can be rewritten as

$$\begin{cases} \partial\bar{U}/\partial t = \bar{V} \\ \partial\bar{V}/\partial t = L_9\bar{U} + I_9\bar{F} \end{cases}, \tag{7}$$

where the spatial differential operator matrix L_9 is defined by

$$L_9 = \begin{pmatrix} D & O & O \\ O & D & O \\ O & O & D \end{pmatrix}_{9 \times 9} \quad ,$$

and I_9 is defined by

$$I_9 = \begin{pmatrix} I & O & O \\ O & I & O \\ O & O & I \end{pmatrix}_{9 \times 9} \quad ,$$

in which I are 3x3 unit matrices.

Eighth-order NAD-SPRK method for the 2D elastic wave

Apparently, eq. (7) satisfies the Hamiltonian system (1), so we consider to solve eq. (7) by the idea of solving the Hamiltonian system. The first step towards solving eq. (7) is to discretize the spatial operator matrix L_9 included in the right-hand side of eq. (7). Here, we use the local interpolation method to approximate the second- and third-order spatial derivatives of wave displacement $u = (u_1, u_2, u_3)$ and particle-velocity $v = (v_1, v_2, v_3)$ included in the right-hand side of eq. (7) by using the wave displacement, the particle-velocity and their gradients at the grid point (i, j) and their neighboring grid points. These computational formulae of the high-order nearly-analytic discrete operators (Tong et al., 2013; Zhang et al., 2014a, 2014b) for approximating the second- and third-order derivatives are listed in the Appendix in detail.

After the discretization of the spatial operator matrix L_9, eq. (7) is converted to a system of semi-discrete Hamiltonian system with respect to time. We then apply the following second-order symplectic partitioned Runge-Kutta method (Sun, 1997) [formula (2) or (3)] to solve the semi-discrete Hamiltonian system (7)

$$\begin{cases} \bar{V}_1 = \bar{V}^n + \tfrac{1}{2}\Delta t L_9 \bar{U}^n \\ \bar{U}^{n+1} = \bar{U}^n + \Delta t \bar{V}_1 \\ \bar{V}^{n+1} = \bar{V}_1 + \tfrac{1}{2}\Delta t L_9 \bar{U}^{n+1} \end{cases} \quad , \tag{8}$$

or

$$\begin{cases} \bar{U}^{n+1} = \bar{V}^n + \Delta t \bar{V}^n + \tfrac{1}{2}\Delta t^2 L_9 \bar{U}^n \\ \bar{V}^{n+1} = \bar{V}^n + \Delta t L_9 \bar{U}^n + \tfrac{1}{2}\Delta t^2 L_9 \bar{V}^n + \tfrac{1}{4}\Delta t^3 L_9^2 \bar{U}^n \end{cases} \quad , \tag{9}$$

where $L_9^2 = L_9 \cdot L_9$.

Eqs. (8) or (9) are called the eighth-order NAD-SPRK method. Owing to using the Taylor series expansion, the errors of $\partial^{m+l}u/\partial x^m \partial z^l$ ($2 \leq m+l \leq 3$) are $O(\Delta x^8 + \Delta z^8)$ by using the interpolation formulae presented in the reference (Tong et al., 2013). In other words, the eighth-order NAD-SPRK method is an eighth-order accuracy scheme in space for the 2D case. When the second-order symplectically partitioned Runge-Kutta method is used to solve the Hamiltonian system (7), the temporal derivative error should be $O(\Delta t^2)$. Therefore, the theoretical errors of the eighth-order NAD-SPRK method for the 2D elastic wave case are $O(\Delta t^2 + \Delta x^8 + \Delta z^8)$.

STABILITY ANALYSIS

As we all know, the temporal increment must satisfy the stability condition of the eighth-order NAD-SPRK method. In our recent work (Zhang et al., 2014b), we have obtained the following stability condition for a 2D acoustic case

$$\Delta t \leq \alpha_{max}(h/c_0) \approx 0.3828(h/c_0) \quad , \tag{10}$$

where $h = \Delta x = \Delta z$ in eq. (10) denotes the space increment. α_{max} is the maximum value of the Courant number defined by $\alpha = c_0 \Delta t / \Delta x$ with the acoustic velocity c_0.

As for the elastic case, it is usually complex to derive the exact or analytical stability condition of a numerical scheme for elastic wave equations (Dong et al, 2000). When the eighth-order NAD-SPRK method is applied to solve the 2D elastic wave equation, the stability condition, which is estimated by the frozen coefficients technique (Vichnevetsky, 1979), can not be directly determined and is approximately correct for the elastic case if the maximal value of the wave velocity is used. Therefore, we estimate that the temporal grid size should satisfy the following stability condition

$$\Delta t \leq \Delta t_{max} \approx 0.3828(h/c_{max}) \quad , \tag{11}$$

where t_{max} is the maximum temporal increment that keeps the eighth-order NAD-SPRK method stable for 2D case, and c_{max} is the maximum P-wave velocity.

NUMERICAL DISPERSION

As we all know, the numerical dispersion is the major artifact when we use FD schemes to model elastic wave-fields. In the section, we investigate the

numerical dispersion of the eighth-order NAD-SPRK method by modeling wavefields. For this purpose, we consider the following 2D elastic wave equations in a homogenous isotropic medium

$$\begin{cases} \rho(\partial^2 u_1/\partial t^2) = (\lambda+2\mu)(\partial^2 u_1/\partial x^2) + \mu(\partial^2 u_1/\partial z^2) + (\lambda+\mu)(\partial^2 u_3/\partial x\partial z) + f_1 \\ \rho(\partial^2 u_3/\partial t^2) = (\lambda+\mu)(\partial^2 u_1/\partial x\partial z) + \mu(\partial^2 u_3/\partial x^2) + (\lambda+2\mu)(\partial^2 u_3/\partial z^2) + f_3 \end{cases}, \quad (12)$$

where u_1, u_3 denote the displacement components in the x- and z-directions, respectively. λ, μ are Lamé parameters, ρ is the medium density, f_1 and f_3 are the force sources of components in the x- and z-directions.

In this numerical experiment, we choose $\lambda = 6.0$ GPa, $\mu = 24.0$ GPa and $\rho = 1.5$ g/cm^3. The number of grid points is 301×301, the spatial grid increments are $\Delta x = \Delta z = 40$ m, and the time increment is $\Delta t = 1 \times 10^{-3}$ s. The source, $f_1 = f(t)$ and $f_3 = 0$, which is located at the center of the computation domain, is a Ricker wavelet with the frequency of f_0. The receiver is located at R(5.25 km, 4.8 km). Here, the Ricker wavelet has the following expression

$$f(t) = -5.76f_0^2[1 - 16(0.6f_0t - 1)^2] \times \exp[-8(0.6f_0t - 1)^2] \quad . \quad (13)$$

Fig. 1 shows the waveforms at the receiver R from T = 0 to T = 0.68s on the frequency of $f_0 = 25$ Hz computed by the eighth-order NAD-SPRK method, the fourth-order NSPRK method, the eighth-order LWC method and the eighth-order SG method, respectively. We can observe that the waveforms in Figs. 1(a), 1(b) and 1(d) are almost identical, whereas the eighth-order LWC method suffers from some numerical dispersion [see Fig. 1(c)].

Fig. 2 also shows the waveforms at receiver R from T = 0 to T = 0.68s generated using these four methods. But the frequency of $f_0 = 40$ Hz is chosen here. From Figs. 2(c) and 2(d), we can see that even the eighth-order LWC and the eighth-order SG methods suffer serious numerical dispersions. However, Figs. 2(a) and 2(b), computed by the eighth-order NAD-SPRK and the fourth-order NSPRK methods, show clear waveforms and they do not show much numerical dispersion for the higher frequency. Especially Fig. 2(a) computed by the eighth-order NAD-SPRK method shows almost no visible numerical dispersion in such a high frequency case. It demonstrates that the eighth-order NAD-SPRK method is more efficient than the high-order methods such as the eighth-order LWC and the eighth-order SG methods in suppressing the numerical dispersion.
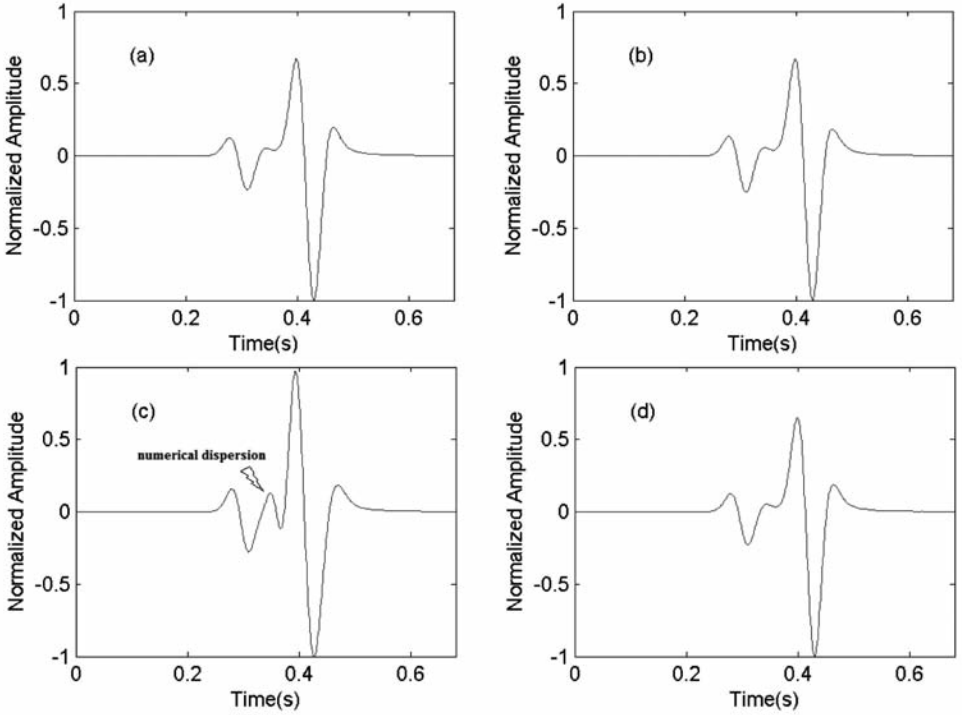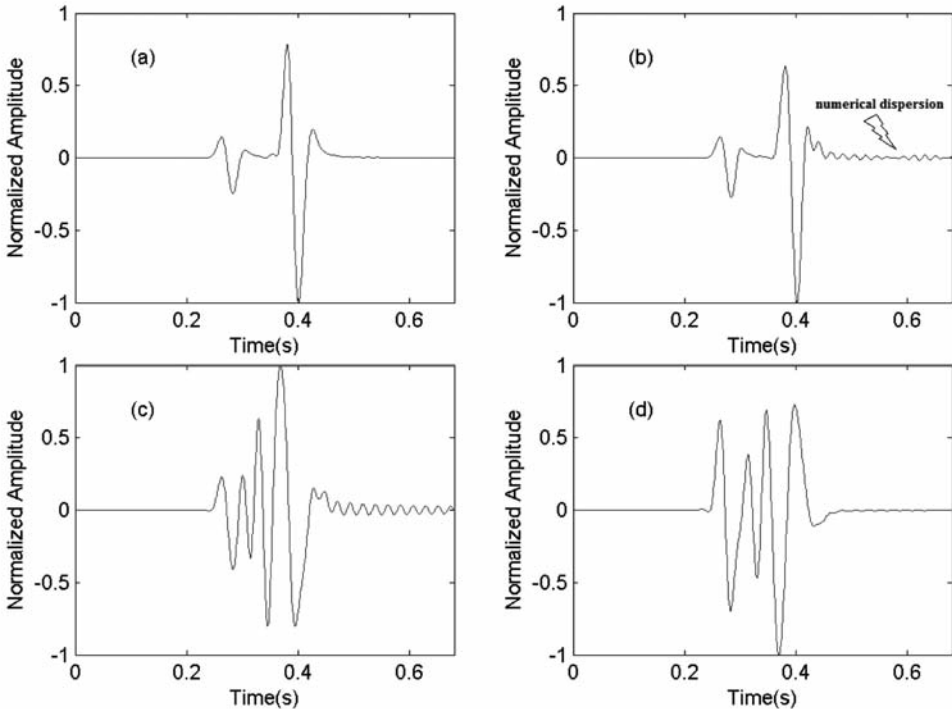
Fig. 1. The waveforms generated by (a) the eighth-order NAD-SPRK method, (b) the fourth-order NSPRK method, (c) the eighth-order LWC method, and (d) the eighth-order SG method, for the homogenous isotropic medium and the Ricker wavelet with the frequency of $f_0 = 25$ Hz.

COMPUTATIONAL EFFICIENCY

In this section, we present the computational results and investigate the computational efficiency of the eighth-order NAD-SPRK method. For this case, we select the same elastic wave equations in a 2D homogenous isotropic medium as eq. (12).

In this experiment, we choose $\lambda = 4.704$ GPa, $\mu = 8.4$ GPa and $\rho = 2.1$ g/cm^3. The number of grid points is 301×301, the spatial grid increments are $\Delta x = \Delta z = 40$ m, and the time increment is $\Delta t = 0.004$ s. The source, which is located at the center of the computation domain, is a Ricker wavelet with a frequency of $f_0 = 12$ Hz. The source functions are $f_1 = f(t)$ and $f_3 = 0$.

Fig. 2. The waveforms generated by (a) the eighth-order NAD-SPRK method, (b) the fourth-order NSPRK method, (c) the eighth-order LWC method, and (d) the eighth-order SG method, for the homogenous isotropic medium and the Ricker wavelet with the frequency of $f_0 = 40$ Hz.

Fig. 3 shows the x-component snapshots (a, b) and z-component snapshots (c, d) at T = 1.6 s on the coarse grid of $\Delta x = \Delta z = 40$ m, generated respectively by the eighth-order NAD-SPRK method (a, c) and the eighth-order LWC method (b, d). From Fig. 3, we can observe that the wave-fronts of elastic waves simulated by these two methods are basically identical, though the computational cost of the eighth-order NAD-SPRK method is more expensive than the eighth-order LWC method for the same number of grid points because more variables including displacement, particle-velocity, and their gradients are simultaneously calculated in the eighth-order NAD-SPRK method. However, the snapshots [see Figs. 3 (a, c)] generated by the eighth-order NAD-SPRK method have much less numerical dispersion even though the spatial size is 40 m, whereas the eighth-order LWC method suffers from serious numerical dispersions [see Figs. 3 (b, d)]. It indicates that the eighth-order NAD-SPRK method can be used to simulate large-scale models with coarse grids.
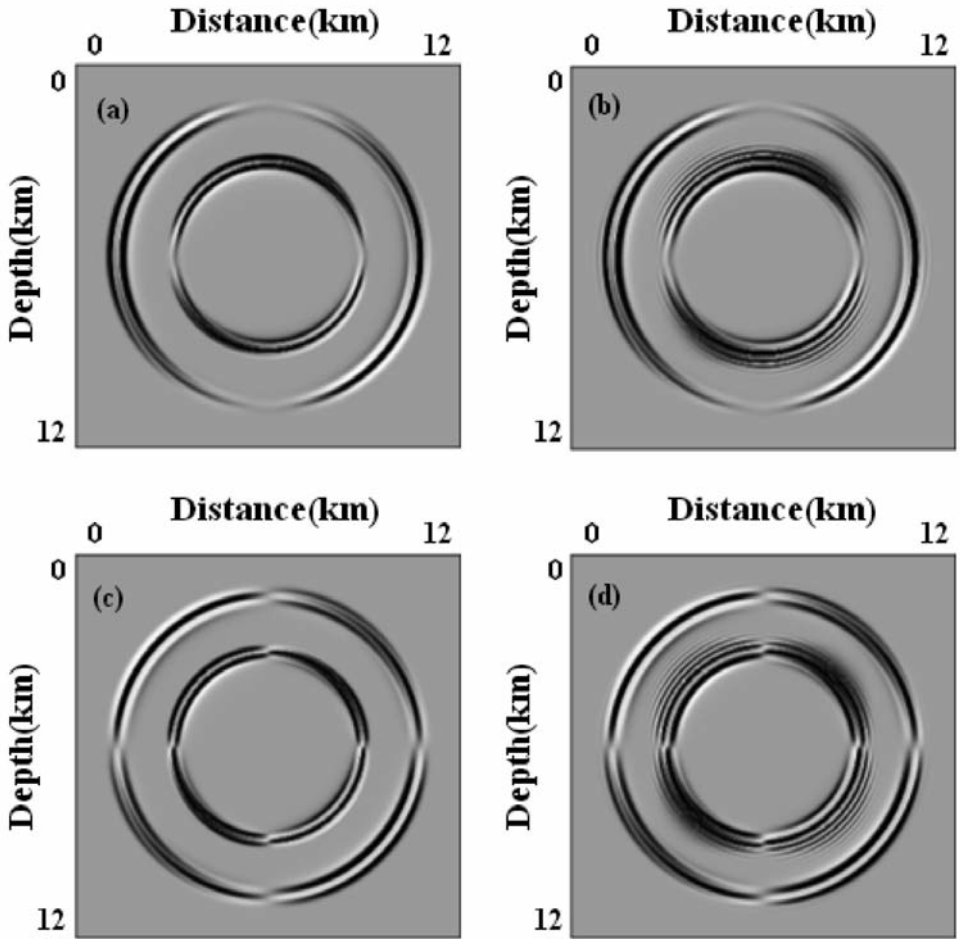
Fig. 3. Snapshots of elastic wave fields at time 1.6 s on the coarse grid of $\Delta x = \Delta z = 40$ m, generated by the eighth-order NAD-SPRK method (a,c) and the eighth-order LWC method (b,d), (a) and (b) delegate the horizontal component, (c) and (d) delegate the vertical component.

For exactly eliminating the numerical dispersion, Fig. 4 generated by the eighth-order LWC method shows the x-component snapshot (a) and z-component snapshot (b) at T = 1.6 s under the same Courant number with the Fig. 3 and on a fine grid of $\Delta x = \Delta z = 20$ m, corresponding to the numbers of grid points of 601×601. While for the same computational domain, the number of mesh points for the eighth-order NAD-SPRK method is only 301×301 on the coarse grid of $\Delta x = \Delta z = 40$ m. As a result, the memory requirement of the eighth-order NAD-SPRK method is approximately 25.08% of that of the eighth-order LWC method.
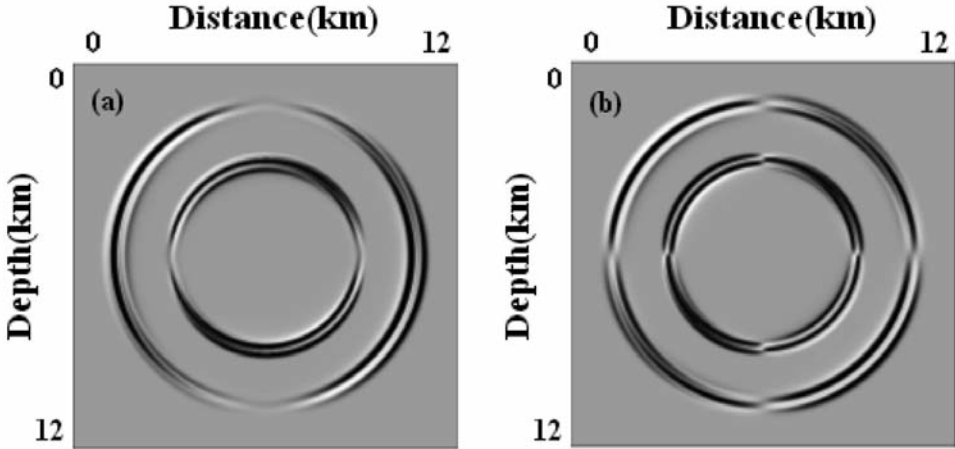
Fig. 4. Snapshots of elastic wave fields at time 1.6 s on the fine grid of $\Delta x = \Delta z = 20$ m, generated by the eighth-order LWC method, (a) delegate horizontal component, (b) delegate vertical component.

Comparing Figs. 3(a, c) with Figs. 4(a, b), it demonstrates that our proposed method can provide the same accuracy as the eighth-order LWC method on a fine grid under the same Courant number. But their computational costs are different. It took the eighth-order NAD-SPRK method about 185 s to generate Figs. 3 (a, c), whereas it took the eighth-order LWC method about 293s to generate Figs. 4 (a, b). It suggests that the computational efficiency of the eighth-order NAD-SPRK method is about 1.6 times of that of the eighth-order LWC method on a fine grid to achieve the same accuracy with no visible wave-field dispersion. Note that our all numerical experiments are performed on a 2-core Pentium-4 computer with 2.33 GB memory.

To investigate the validity of the eighth-order NAD-SPRK method, we compare the numerical solutions computed by the eighth-order NAD-SPRK method with the eighth-order LWC method for the 2D elastic wave equations. Because Dablain in his study (1986) has demonstrated that the eighth-order LWC method on fine grids can provide accurate results, which are similar to the analytic solution and equivalent with the pseudo spectral method.

The spatial and temporal increments are chosen as $\Delta x = \Delta z = 40$ m and $\Delta t = 0.004$ s for the eighth-order NAD-SPRK method, whereas much finer space and time grids of $\Delta x = \Delta z = 20$ m and $\Delta t = 0.002$ s are needed for the eighth-order LWC method to produce an approximately equivalent result. Fig.5

shows the waveforms generated by the eighth-order NAD-SPRK method on the coarse grids ($\Delta x = \Delta z = 40$ m) and the eighth-order LWC method on the fine grids ($\Delta x = \Delta z = 20$ m) in modeling the elastic wave, where Figs. 5(a) and 5(b) are those of the horizontal and vertical displacement component at receiver R(6.6 km, 7.6 km), respectively. Comparison of these figures indicates that the eighth-order NAD-SPRK method can provide the equivalent solutions on much coarser grids for a homogeneous isotropic model, which requires much less computation and computer memory.
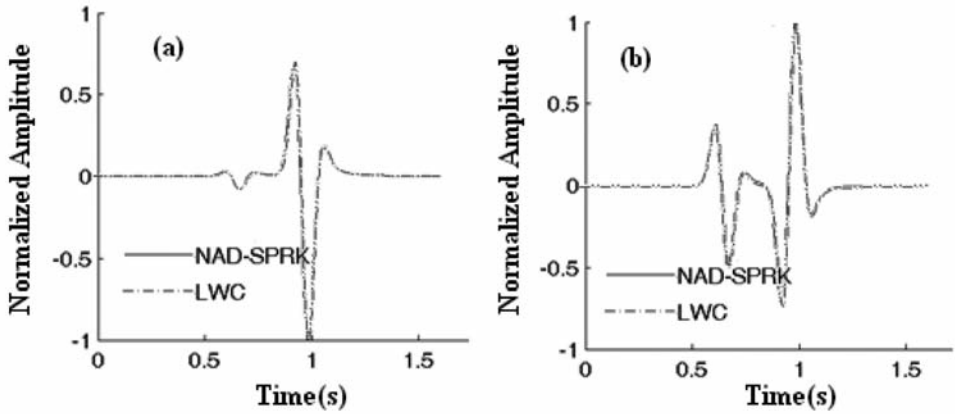
Fig. 5. Comparisons of waveforms for (a) horizontal displacement component, (b) vertical displacement component at receiver R(6.6 km, 7.6 km), generated by the eighth-order LWC method (dashed line) on the fine grids ($\Delta x = \Delta z = 20$ m and $\Delta t = 0.002$ s) and the eighth-order NAD-SPRK method (solid line) on the coarse grids ($\Delta x = \Delta z = 40$ m and $\Delta t = 0.004$ s), respectively.

NUMERICAL SIMULATIONS

In order to further investigate the computational efficiency and the numerical dispersion of the eighth-order NAD-SPRK method, we apply this method to simulate 2D elastic waves propagating in homogeneous transversely isotropic medium, two-layer homogeneous isotropic medium, two-layer heterogeneous medium and three-layer medium with a fluctuating interface.

Homogeneous transversely isotropic model

Firstly, we simply simulate the elastic waves propagating in the homogeneous transversely isotropic medium for the 2D case. We choose the wave equations as follows

$$\begin{cases} \rho(\partial^2 u_1/\partial t^2) = c_{11}(\partial^2 u_1/\partial x^2) + c_{44}(\partial^2 u_1/\partial z^2) + (c_{13}+c_{44})(\partial^2 u_3/\partial x\partial z) + f_1 \\ \rho(\partial^2 u_3/\partial t^2) = (c_{13}+c_{44})(\partial^2 u_1/\partial x\partial z) + c_{44}(\partial^2 u_3/\partial x^2) + c_{33}(\partial^2 u_3/\partial z^2) + f_3 \end{cases}, \quad (14)$$

where u_1, u_3 denote the displacement components in the x- and z-directions, respectively. c_{11}, c_{13}, c_{33} and c_{44} are elastic constants, ρ is the medium density, f_1 and f_3 are the force source components in the x- and z-directions.

   In this numerical example, we take the parameters of c_{11} = 26.4 GPa, c_{13} = 6.11 GPa, c_{33} = 15.6 GPa, c_{44} = 4.8 GPa and ρ = 2.1 g/cm³. The source, which is located at the center of the computational domain, is a Ricker wavelet $f_1 = f_3 = f(t)$ with the frequency of f_0 = 12 Hz. The computational domain is $0 \le x \le 6$ km, $0 \le z \le 6$ km. The spatial and temporal increments are $\Delta x = \Delta z = 30$ m, $\Delta t = 0.0008$ s, respectively. The receivers are located at R_1(2.5km, 3.0km) and R_2(2.5km, 2.5km), respectively.

   Fig. 6, generated by the eighth-order NAD-SPRK method, shows the snapshots of the x- and z-directions displacement component at time T = 0.9s. Fig.7, generated by the eighth-order NAD-SPRK method, shows the wave seismograms of the horizontal displacement component at receiver R_1 and R_2 from T = 0 to T = 0.9 s. From Figs. 6 and 7, we can see that the eighth-order NAD-SPRK method shows very clear results and has no visible numerical dispersion. It suggests that the eighth-order NAD-SPRK method can be efficient to suppress the numerical dispersions and can provide the accurate results for the elastic wave modeling in homogeneous transversely isotropic medium of the 2D case.
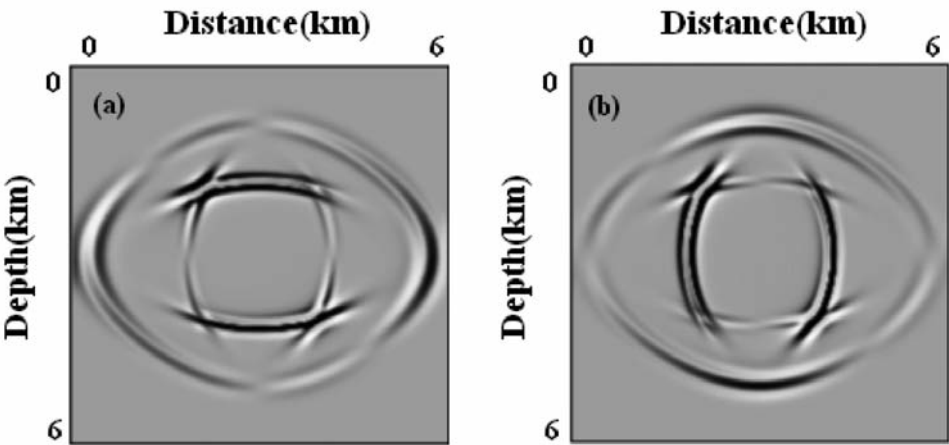

Fig. 6. Snapshots of elastic wave fields for the homogeneous transversely isotropic model at time 0.9 s, generated by the eighth-order NAD-SPRK method, (a) delegates the horizontal displacement component, (b) delegates the vertical displacement component.
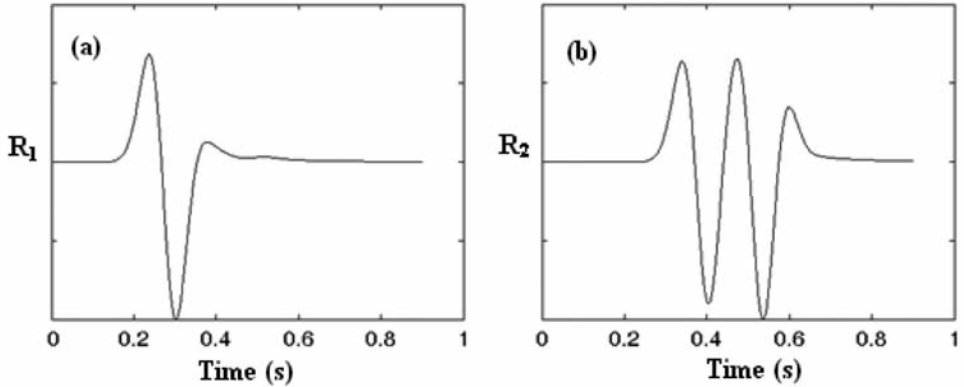
Fig. 7. Elastic wave seismograms for horizontal displacement component at receiver R_1(a) and R_2(b), generated by the eighth-order NAD-SPRK method.

Two-layer homogeneous isotropic model

Secondly, we simulate the elastic wave [see eq. (12)] propagating through a two-layer homogenous isotropic medium for the 2D case. The size of the computational domain is $0 \leq x,z \leq 9.6$ km and the horizontal interface is at the depth of $z = 3.84$ km. We take the Lamé parameters and densities of $\lambda_1 = 1.12$ GPa, $\mu_1 = 2.592$ GPa and $\rho_1 = 1.8$ g/cm^3 in the upper part, and $\lambda_2 = 7.35$ GPa, $\mu_2 = 13.125$ GPa and $\rho_2 = 2.1$ g/cm^3 in the lower layer, respectively. The explosive source, $f_1 = f(t)$ and $f_3 = 0$, of the Ricker wavelet with a frequency $f_0 = 14$ Hz is located at $O(4.8$km, 3.12 km). Spatial and temporal increments are chosen as $\Delta x = \Delta z = 30$ m and $\Delta t = 0.0032$ s.

Fig. 8 shows the snapshots of the x-direction displacement component at time $T = 1.5$ s generated by the eighth-order NAD-SPRK method, the fourth-order NSPRK method, the eighth-order LWC method and the eighth-order SG method, respectively. From Figs. 8(b), (c), and (d), we can see that the results of the fourth-order NSPRK, the eighth-order LWC, and the eighth-order SG methods show serious numerical dispersion in the low-velocity layer and at the strong interface, whereas Fig. 8(a) generated by the eighth-order NAD-SPRK method shows very clear result and has no visible numerical dispersion even for the large vertical velocity contrast.
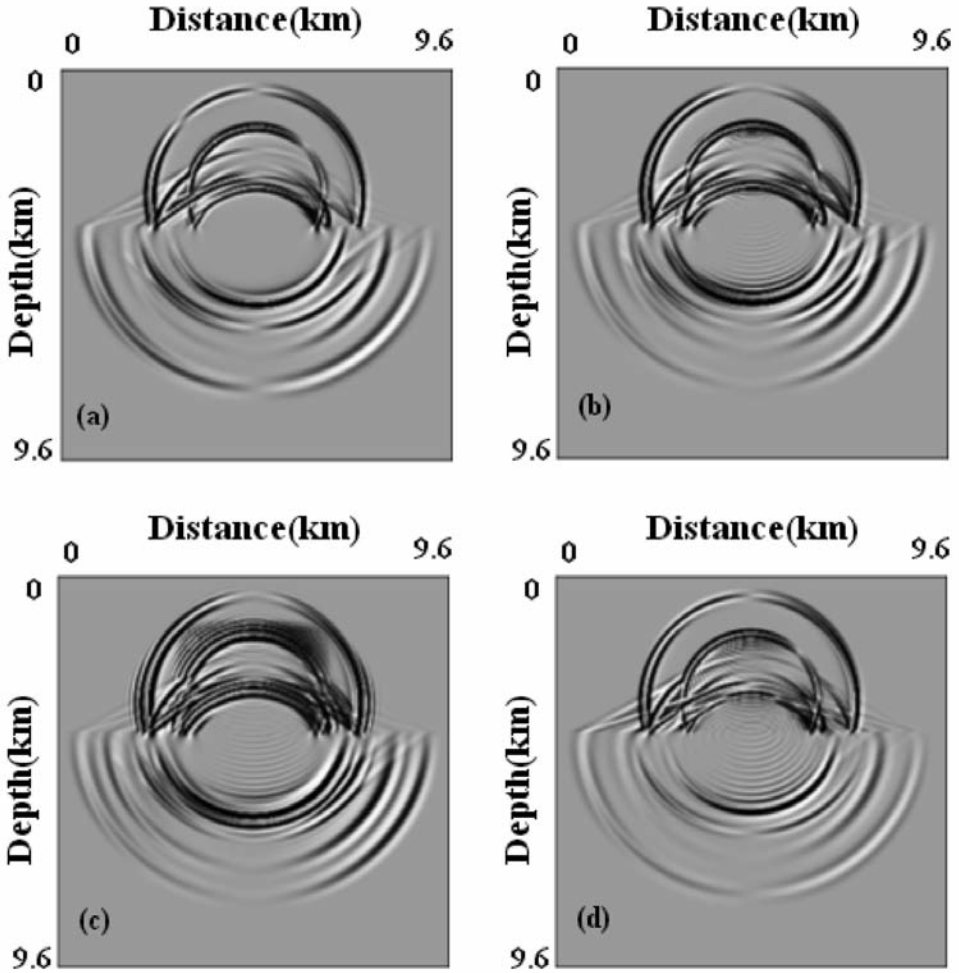
Fig. 8. Snapshots of elastic wave fields for the two-layer model at time 1.5 s, (a), (d), (b) and (c) delegate horizontal displacement component, generated by the eighth-order NAD-SPRK method, the fourth-order NSPRK method, the eighth-order LWC method, the eighth-order SG method, respectively.

Two-layer heterogeneous model

In order to further investigate the availability of the eighth-order NAD-SPRK method in simulating the seismic propagating through the heterogeneous medium, we select the two-layer medium model of the 2D case with the top layer of the isotropic medium and the bottom layer of the VTI

medium. We take the elasticity coefficients and densities of $\lambda = 4.8$ GPa, $\mu = 6.5$ GPa, and $\rho_1 = 3.2$ g/cm^3 in the top layer, and $c_{11} = 40.8$ GPa, $c_{13} = 13.2$GPa, $c_{33} = 50.6$ GPa, $c_{44} = 25$ GPa, and $\rho_2 = 4.2$ g/cm^3 in the bottom layer, respectively. The computational domain is $0 \leq x \leq 6$ km and $0 \leq x \leq 6$ km and the horizontal interface at the depth of $z = 3.0$ km. The explosive source, with a frequency of $f_0 = 25$ Hz, is located at O(3km, 2.76km). The spatial and temporal increments are chosen as $\Delta x = \Delta z = 20$ m and $\Delta t = 0.002$ s, respectively. The source function is $f_1 = f_3 = f(t)$.
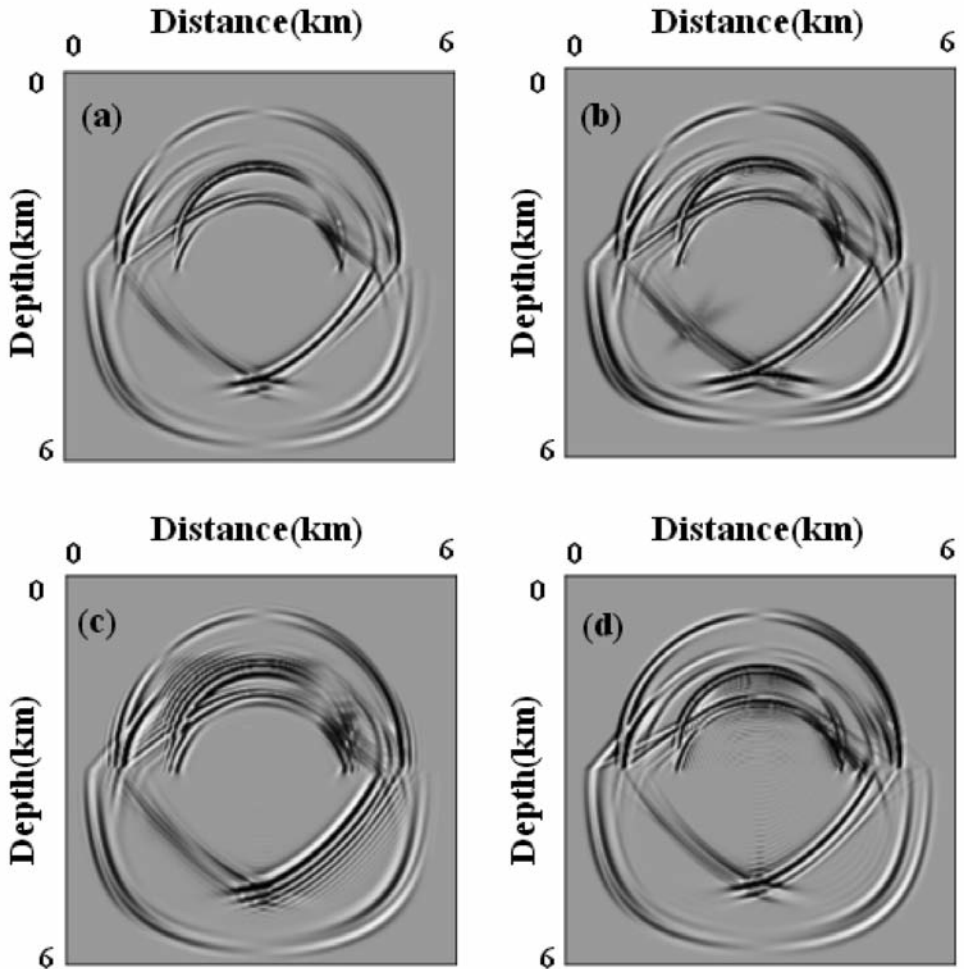

Fig. 9. Snapshots of elastic wave fields for horizontal displacement component for the two-layer heterogeneous model at time 0.96 s, generated by (a) the eighth-order NAD-SPRK method, (b) the fourth-order NSPRK method, (c) the eighth-order LWC method, and (d) the eighth-order SG method, respectively.

Fig. 9 shows the wave-field snapshots for the horizontal displacements in the x-direction and Fig. 10 shows the vertical displacements in the z-direction at time T = 0.96 s for the two-layer heterogeneous elastic medium model on the grids of $\Delta x = \Delta z = 20$ m, generated by the eighth-order NAD-SPRK method, the fourth-order NSPRK, the eighth-order LWC method, and the eighth-order SG method, respectively. From Fig. 9(a) and Fig. 10(a) computed by the eighth-order NAD-SPRK method, we can observe that numerous phases such as direct P-wave, direct S-wave, and their reflected, transmitted, and converted phases from the inner interface are very clear, and show no visible
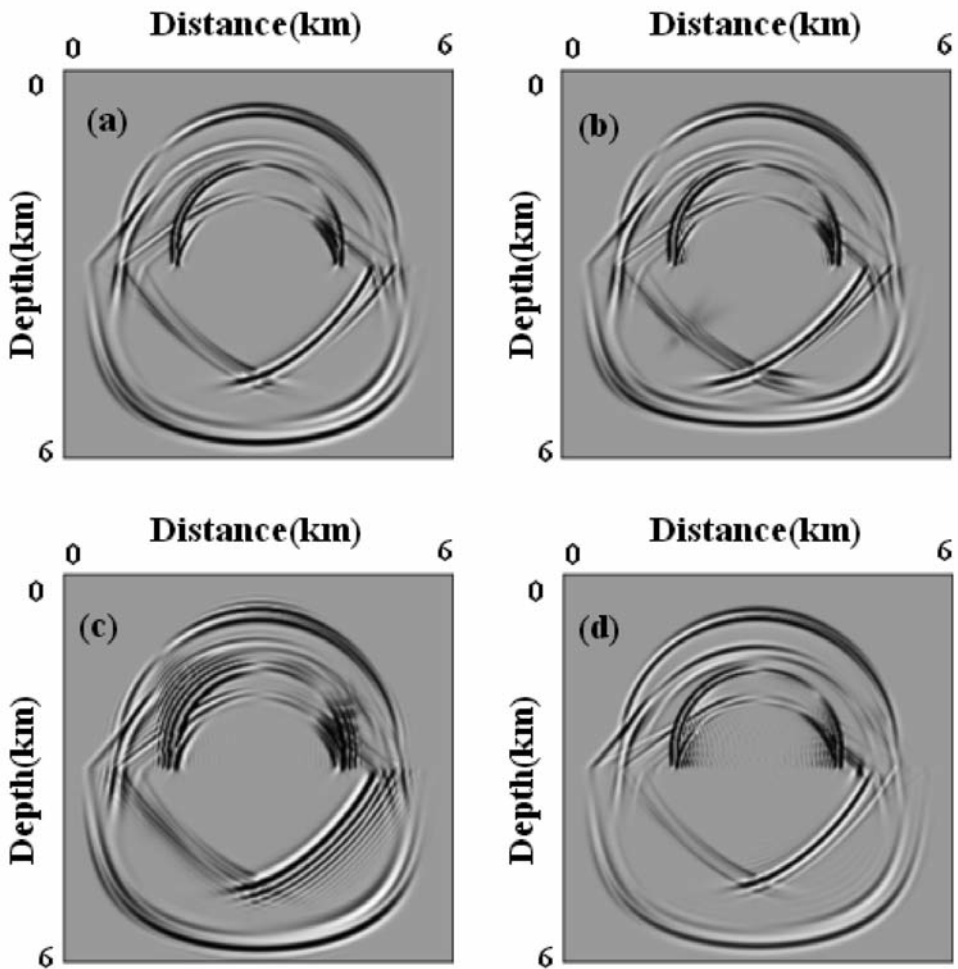

Fig. 10. Snapshots of elastic wave fields for vertical displacement component for the two-layer heterogeneous model at time 0.96 s, generated by (a) the eighth-order NAD-SPRK method, (b) the fourth-order NSPRK method, (c) the eighth-order LWC method, and (d) the eighth-order SG method, respectively.

numerical dispersion. However, the snapshots generated by the fourth-order NSPRK [Fig. 9(b) and Fig. 10(b)] and the eighth-order SG method [Fig. 9(d) and Fig. 10(d)] show small numerical dispersion, and the eighth-order LWC method suffers from serious numerical dispersion [Fig. 9(c) and Fig. 10(c)]. It demonstrates that the eighth-order NAD-SPRK method is very effective in suppressing numerical dispersion for the two-layer elastic model of heterogeneous medium.

Three-layer model with a fluctuating interface

In our last numerical experiment, we choose a three-layer model shown in Fig. 11, which includes a low-velocity thin layer in the middle and an irregular interface between the middle and bottom layers. The P-wave velocity, S-wave velocity, and density in the top and bottom layers are V_P = 4.0 km/s, V_S = 2.309 km/s, and ρ = 2.3 g/cm^3, respectively, whereas in the middle thin layer V_P = 2.0 km/s, V_S = 1.155 km/s, and ρ = 2.0 g/cm^3, which shows a velocity contrast between the adjacent layers to reach more than twice. The explosive source with a frequency of f_0 = 15 Hz is located at the centre of the computational domain. The temporal and spatial increments are chosen at Δt = 1 ms and Δx = Δz = 20 m, respectively. In this experiment, we use the classical split perfectly matched layer (PML) (Dimitri and Jeroen, 2003) as the absorbing boundary condition to eliminate the reflections at the artificial boundaries.
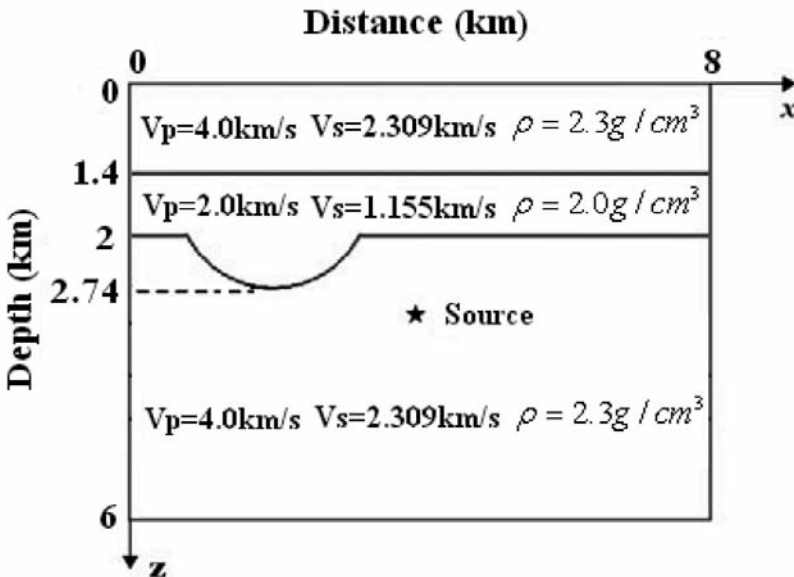

Fig. 11. Three-layer model with a fluctuating interface.

Fig. 12 shows the snapshots of the horizontal component at T = 0.6 s
[Fig. 12(a)], T = 0.8 s [Fig. 12(b)], T = 1.0 s [Fig. 12(c)], T = 1.2 s
[Fig.12(d)], respectively. Figs. 12(a-d) are clear and have no visible numerical
dispersion, which shows that the eighth-order NAD-SPRK method can keep the
physical properties of elastic wave propagating in a multilayer medium and can
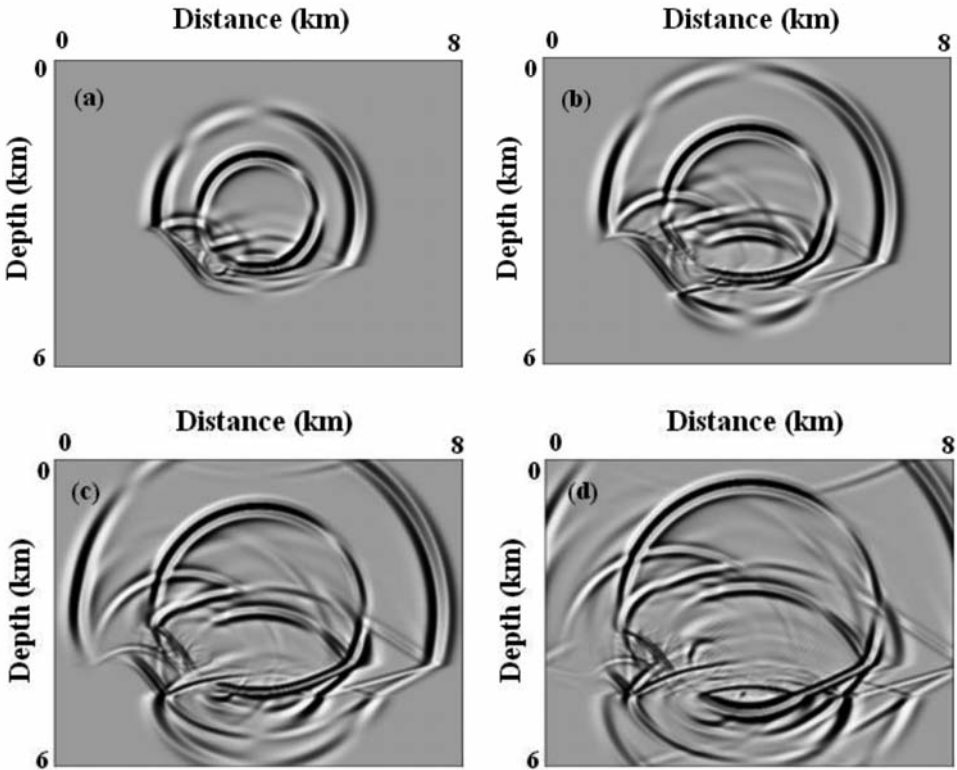effectively suppress the numerical dispersion.

Fig. 12. Snapshots of elastic wave fields for the horizontal component at different times of (a) T =
0.6 s, (b) T = 0.8 s, (c) T = 1.0 s, and (d) T = 1.2 s. The PML absorbing boundary condition
is used in this experiment.

Figs. 13(a) and (b), respectively, show the horizontal seismograms of the
horizontal and vertical displacement components from 0 to 1.4 s at receivers
spaced 20 m apart on the horizontal plane of z = 6 km spreading from 0 to 8
km at the location of (8km, 6km). Figs. 14(a) and (b), respectively, show the
vertical seismic profiles of the horizontal and vertical displacement components
from 0 to 1.4 s at receivers spaced 20 m apart on the vertical plane of x = 8
km spreading from 0 to 6 km at the location of (8km, 6km).

In those figures of Fig. 12(c,d), Fig. 13 and Fig. 14, the waveforms of the reflected waves are clear and there is no visible numerical dispersion, which demonstrates that the PML condition can effectively absorb the reflected waves from the artificial boundaries. This experiment illustrates that it is successful and effective for the eighth-order NAD-SPRK method to be combined with the PML absorbing boundary condition.
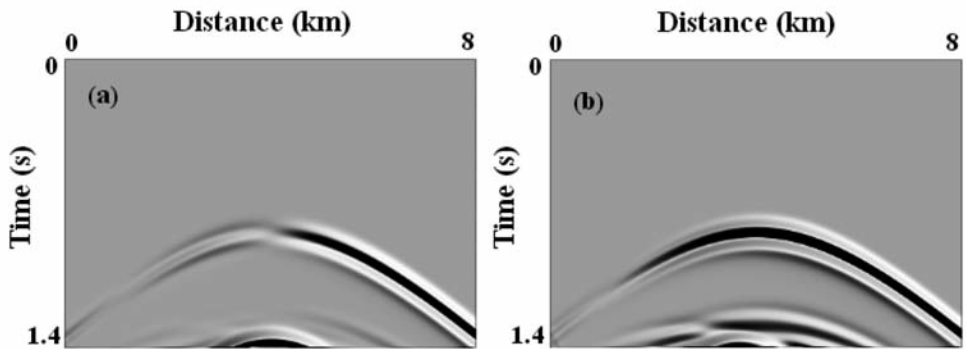

Fig. 13. Horizontal seismograms of elastic wave fields from 0 to 1.4 s for (a) the horizontal component and (b) the vertical component of the elastic wave displacement.
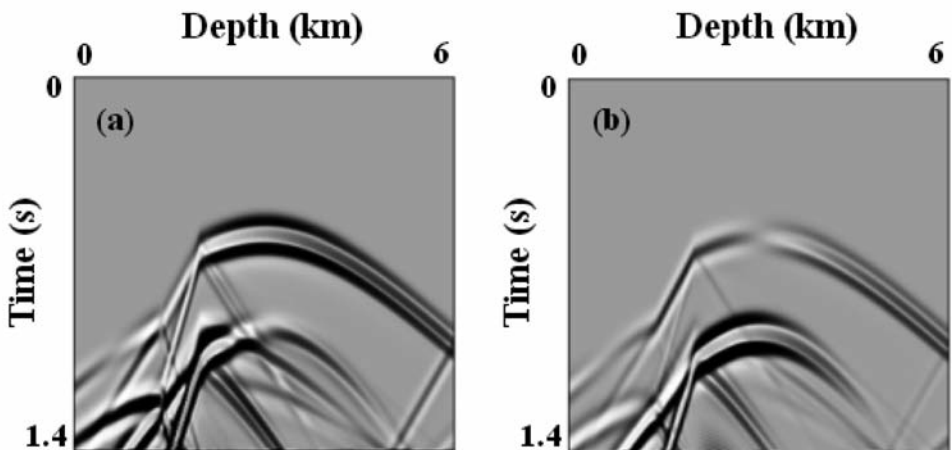

Fig. 14. Vertical seismic records of elastic wave fields from 0 to 1.4 s for (a) the horizontal component and (b) the vertical component of the elastic wave displacement.

DISCUSSION AND CONCLUSIONS

The computational cost and the memory storage are two important problems of common concern in 2D wave-propagation modeling using the FD methods. The FD methods need oversampling in order to eliminate the serious numerical dispersion caused by the discretization to the wave equations. In the paper, we propose the eighth-order NAD-SPRK method for solving the 2D elastic wave equations, which can effectively suppress the numerical dispersion through using the fewer sampling points per minimum wavelength. The 2D elastic wave equations are first transformed into the Hamiltonian system, and then the time derivatives are approximated using the second-order symplectic partitioned Runge-Kutta method, while the space derivatives are calculated using the nearly analytic discrete operator with the eighth-order accuracy. So the eighth-order NAD-SPRK method is second-order accurate in time and eighth-order accurate in space. The approximating formulae listed in the Appendix are dependent on the values of the displacement and the particle velocity, together with their gradients. As a result, the eighth-order NAD-SPRK method can effectively suppress the numerical dispersion using few sampling points per minimum wavelength.

We give the stability criteria (11) of the eighth-order NAD-SPRK method for solving the 2D elastic equations. Numerical examples demonstrate that the eighth-order NAD-SPRK method is more efficient than the high-order methods such as the fourth-order NAD-SPRK method, the eighth-order LWC method, and the eighth-order SG method in suppressing the numerical dispersion [see Figs. 1-2].

Our numerical experiments show computational costs and memory requirements for the eighth-order NAD-SPRK method are much less than those of the eighth-order LWC method. To achieve the same results with no visible numerical dispersion [see Figs. 3-4], the computational speed of the eighth-order NAD-SPRK method is approximately 1.6 times that of the eighth-order LWC method, and the memory required for the eighth-order NAD-RK method is about 25.08% of the eighth-order LWC method. Against the eighth-order LWC method, comparison results indicate that the eighth-order NAD-SPRK method can provide the equivalent solutions on much coarser grids with analytic solutions [see Fig. 5].

Wave-field modeling, shown in Figs. 6, 7, 8, 9, 10, 12, 13 and 14, further confirms our conclusion that the eighth-order NAD-SPRK method has much less numerical dispersion even for the fewer space-sampling points per minimum wavelength or larger velocity contrasts between adjacent layers. Meanwhile, it shows that the new method can greatly save the computer memory and improve the calculation speed. Specially, we incorporate the PML condition into the eighth-order NAD-SPRK method, and numerical experiments

show the calculation is successful and effectively in absorbing the artificial boundary reflections. These numerical results imply that simultaneously using both the wave displacement and its gradients to approximate the high-order spatial derivatives is important for both reducing the numerical dispersion and compensating the important wave-field information included in the displacement and particle velocity gradients.

In summary, the eighth-order NAD-SPRK method has a very good effect in suppressing the numerical dispersion, and can preserve the symplectic structure of the Hamiltonian system because of the using of the symplecticity-conserving method for time derivatives. Therefore, as a numerical computational method, the eighth-order NAD-SPRK method has a tremendous application potentiality in the seismic exploration area and seismology research. At the same time, because of its symplecticity-conserving property, it is potentially useful to perform applications in large-scale seismic modelling as well as in seismic migration based on wave equations.

ACKNOWLEDGEMENTS

REFERENCES

Chen, K.H., 1984. Propagating numerical model of elastic wave in anisotropic in homogeneous media-finite element method. Expanded Abstr., 54th Ann. Internat. SEG Mtg., Atlanta: 631-632.

Chen, S., Yang, D.H. and Deng, X.Y., 2010. A weighted Runge-Kutta method with weak numerical dispersion for solving wave equations. Commun. Comput. Phys., 7: 1027-1048.

Chen, X.F., 1993. A systematic and efficient method of computing normal modes for multi-layered half space. Geophys. J. Internat., 115: 3912-409.

Dablain, M.A., 1986. The application of high-order differencing to scalar wave equation. Geophysics, 51: 54-66.

Dimitri, K. and Jeroen, T., 2003. A perfectly matched layer absorbing boundary condition for the second-order seismic wave equation. Geophys. J. Internat., 154: 146-153.

Dong, L.G., Ma, Z.T., Cao, J.Z., Wang, H.Z., Gong, J.H., Lei, B. and Xu, S.Y., 2000. A staggered-grid high-order difference method of one-order elastic wave equation. Chin. J. Geophys. (in Chinese), 43: 411-419.

Fei, T. and Larner, K., 1995. Elimination of numerical dispersion in finite difference modeling and migration by flux-corrected transport. Geophysics, 60: 1830-1842.

Huang, B.S., 1992. A program for two-dimensional seismic wave propagation by the pseudo-spectrum method. Comput. Geosci., 18: 289-307.

Kelly, K.R., Wave, R.W. and Treitel, S., 1976. Synthetic seismograms: a finite-difference approach. Geophysics, 41: 2-27.

Komatitsch, D. and Vilotte, J.P., 1998. The spectral element method: an efficient tool to simulate the seismic responses of 2D and 3D geological structures. Bull. Seismol. Soc. Am., 88: 368-392.

Ma, S. and Liu, P., 2006. Modeling of the perfectly matched layer absorbing boundaries and intrinsic attenuation in explicit finite-element methods. Bull. Seismol. Soc. Am., 96: 1779-1794.

Ma, X., Yang, D.H. and Liu, F.Q., 2011. A nearly analytic symplectically partitioned Runge-Kutta method for 2-D seismic wave equations. Geophys. J. Internat., 187: 480-496.

Ma, X., Yang, D.H. and Zhang, J.H., 2010. Symplectic partitioned Runge-Kutta method of solving the acoustic wave equation. Chin. J. Geophys. (in Chinese), 53: 1993-2003.

Moczo, P., Kristek, J. and Halada, L., 2000. 3D 4th-order staggered-grid finite-difference schemes: stability and grid dispersion. Bull. Seismol. Soc. Am., 90: 587-603.

Moczo, P., Kristek, J., Galis, M., Pazak, P. and Balazovjech, M., 2007. The finite-difference and finite-element modeling of seismic wave propagation and earthquake motion. Acta Phys. Slov., 57: 177-406.

Moczo, P., Kristek, J., Vavrýcuk, V., Archuleta, R.J. and Halada, L., 2002. 3D heterogeneous staggered-grid finite-difference modeling of seismic motion with volume harmonic and arithmetic averaging of elastic moduli and densities. Bull. Seismol. Soc. Am., 92: 3042-3066.

Qin, M.Z. and Zhang, M.Q., 1990. Multi-stage symplectic schemes of two kinds of Hamiltonian systems for wave equations. Comput. Math. Appl., 19: 51-62.

Ruth, R.D., 1983. A canonical integration technique. IEEE Trans. Nucl. Sci., NS-30 (4): 2669-2671.

Sänger, E.H., Gold, N. and Shapiro, S.A., 2000. Modeling the propagation of elastic waves using a modified finite-difference grid. Wave Motion, 31: 77-92.

Smith, W.D., 1975. The application of finite element analysis to body wave propagation problems, Geophys. J., 42: 747-768.

Sun, G., 1997. A class of explicitly symplectic schemes for wave equations. Comput. Math. (in Chinese), 1: 1-10.

Tong, P., Yang, D.H., Hua, B.L. and Wang, M.X., 2013. A high-order stereo-modeling method for solving wave equations. Bull. Seismol. Soc. Am., 103: 811-833.

Vichnevetsky, R., 1979. Stability charts in the numerical approximation of partial differential equation: A review. Mathemat. Comput. Simulat., 21: 170-177.

Wang, L., Yang, D.H. and Deng, X.Y., 2009. A WNAD method for seismic stress-field modeling in heterogeneous media. Chin. J. Geophys. (in Chinese), 52: 1526-1535.

Yang, D.H., 2002. Finite element method of the elastic wave equation and wave field simulation in two-phase anisotropic media. Chin. J. Geophys. (in Chinese), 45: 575-583.

Yang, D.H., Liu, E., Zhang, Z.J. and Teng, J.W., 2002. Finite-difference modeling in two-dimensional anisotropic media using a flux-corrected transport technique. Geophys. J. Internat., 148: 320-328.

Yang, D.H., Peng, J.M., Lu, M. and Terlaky, T., 2006. Optimal nearly-analytic discrete approximation to the scalar wave equation. Bull. Seismol. Soc. Am., 96: 1114-1130.

Yang, D.H., Song, G.J., Chen, S. and Hou, B.Y., 2007. An improved nearly analytical discrete method: an efficient tool to simulate the seismic response of 2-D porous structures. J. Geophys. Eng., 4: 40-52.

Yang, D.H., Teng, J.W., Zhang, Z.J. and Liu, E., 2003. A nearly-analytic discrete method for acoustic and elastic wave equations in anisotropic media. Bull. Seismol. Soc. Am., 93:   882-890.

Yang, D.H., Tong, P. and Deng, X.Y., 2012. A central difference method with low numerical dispersion for solving the scalar wave equation. Geophys. Prosp., 60: 885-905.

Yang, D.H., Wang, N., Chen, S. and Song, G.J., 2009. An explicit method based on the implicit Runge-Kutta algorithm for solving the wave equations. Bull. Seismol. Soc. Am., 99: 3340-3354.

Yoshida, H., 1993. Recent Progress in the theory and application of symplectic integrators. Celest. Mech. Dyn. Astr., 56: 27-43.

Zhang, C.Y., Li, X., Ma, X. and Song, G.J., 2014a. A Runge-Kutta method with using eighth-order nearly-analytic spatial discretization operator for solving a 2D acoustic wave equation. J. Seismic Explor., 23: 279-302.

Zhang, C.Y., Ma, X., Yang, L. and Song, G.J., 2014b. Symplectic partitioned Runge-Kutta method based on the eighth-order nearly analytic discrete operator and its wavefield simulations. Appl. Geophys., 11: 89-106.

APPENDIX

APPROXIMATION OF EIGHTH-ORDER DERIVATIVES

In order to obtain the approximation formulae of eighth-order derivatives in eq. (7) for the 2D elastic case, Tong et al. (2013) derived these approximate formulae. For convenience, here we give the approximation formulae of the displacement u as follows

$$\partial^2 u_{j,k}/\partial x^2 = (1/\Delta x^2)[(7/54)(u_{j-2,k}+u_{j+2,k}) + (64/27)(u_{j-1,k}+u_{j+1,k}) -5u_{j,k}]$$

$$+ (1/\Delta x)\{(1/36)[(\partial u_{j-2,k}/\partial x)-(\partial u_{j+2,k}/\partial x)] + (8/9)[(\partial u_{j-1,k}/\partial x)-(\partial u_{j+1,k}/\partial x)]\} \quad , \qquad \text{(A-1)}$$

$$\partial^2 u_{j,k}/\partial z^2 = (1/\Delta z^2)[(7/54)(u_{j,k-2}+u_{j,k+2}) + (64/27)(u_{j,k-1}+u_{j,k+1}) -5u_{j,k}]$$

$$+ (1/\Delta z)\{(1/36)[(\partial u_{j,k-2}/\partial z)-(\partial u_{j,k+2}/\partial z)] + (8/9)[(\partial u_{j,k-1}/\partial z)-(\partial u_{j,k+1}/\partial z)]\} \quad , \qquad \text{(A-2)}$$

$$\partial^2 u_{j,k}/\partial x\partial z = (7/216\Delta x\Delta z)(u_{j-2,k-2} + u_{j+2,k+2} - u_{j-2,k+2} - u_{j+2,k-2})$$

$$+ (16/27\Delta x\Delta z)(u_{j-1,k-1} + u_{j+1,k+1} - u_{j-1,k+1} - u_{j+1,k-1})$$

$$+ (1/144\Delta x)[(\partial u_{j-2,k-2}/\partial z) - (\partial u_{j+2,k+2}/\partial z) + (\partial u_{j-2,k+2}/\partial z) - (\partial u_{j+2,k-2}/\partial z)]$$

$$+ (1/144\Delta z)[(\partial u_{j-2,k-2}/\partial x) - (\partial u_{j+2,k+2}/\partial x) + (\partial u_{j+2,k-2}/\partial x) - (\partial u_{j-2,k+2}/\partial x)]$$

$$+ (2/9\Delta x)[(\partial u_{j-1,k-1}/\partial z) - (\partial u_{j+1,k+1}/\partial z) + (\partial u_{j-1,k+1}/\partial z) - (\partial u_{j+1,k-1}/\partial z)]$$

$$+ (2/9\Delta z)[(\partial u_{j-1,k-1}/\partial x) - (\partial u_{j+1,k+1}/\partial x) + (\partial u_{j+1,k-1}/\partial x) - (\partial u_{j-1,k+1}/\partial x)] \quad , \qquad \text{(A-3)}$$

$$\partial^3 u_{j,k}/\partial x^3 = (1/\Delta x^3)[-(31/144)(u_{j-2,k}-u_{j+2,k}) - (88/9)(u_{j-1,k}-u_{j+1,k})]$$

$$+ (1/\Delta x^2)\{-(1/24)[(\partial u_{j-2,k}/\partial x)+(\partial u_{j+2,k}/\partial x)] - (8/3)[(\partial u_{j-1,k}/\partial x)-(\partial u_{j+1,k}/\partial x)]-15(\partial u_{j,k}/\partial x)\}, \quad \text{(A-4)}$$

$$\partial^3 u_{j,k}/\partial z^3 = (1/\Delta z^3)[-(31/144)(u_{j,k-2}-u_{j,k+2}) - (88/9)(u_{j,k-1}-u_{j,k+1})]$$

$$+ (1/\Delta z^2)\{-(1/24)[(\partial u_{j,k-2}/\partial z)+(\partial u_{j,k+2}/\partial z)] - (8/3)[(\partial u_{j,k-1}/\partial z)-(\partial u_{j,k+1}/\partial z)]-15(\partial u_{j,k}/\partial z)\}, \quad \text{(A-5)}$$

$$\partial^3 u_{j,k}/\partial x\partial z^2 = (31/864\Delta x\Delta z^2)(u_{j+2,k+2} - u_{j-2,k-2} + u_{j+2,k-2} - u_{j-2,k+2} + 2u_{j-2,k} - 2u_{j+2,k})$$

$$+ (44/27\Delta x\Delta z^2)(u_{j+1,k+1} - u_{j-1,k-1} + u_{j+1,k-1} - u_{j-1,k+1} + 2u_{j-1,k} - 2u_{j+1,k})$$

$$-(1/144\Delta z^2)[(\partial u_{j-2,k-2}/\partial x)+(\partial u_{j+2,k+2}/\partial x)+(\partial u_{j-2,k+2}/\partial x)+(\partial u_{j+2,k-2}/\partial x)-2(\partial u_{j+2,k}/\partial x)-2(\partial u_{j-2,k}/\partial x)]$$

$$-(4/9\Delta z^2)[(\partial u_{j-1,k-1}/\partial x)+(\partial u_{j+1,k+1}/\partial x)+(\partial u_{j-1,k+1}/\partial x)+(\partial u_{j+1,k-1}/\partial x)-2(\partial u_{j+1,k}/\partial x)-2(\partial u_{j-1,k}/\partial x)]$$

$$-(1/144\Delta x\Delta z)[(\partial u_{j-2,k-2}/\partial z) + (\partial u_{j+2,k+2}/\partial z) - (\partial u_{j-2,k+2}/\partial z) - (\partial u_{j+2,k-2}/\partial z)]$$

$$-(4/9\Delta x\Delta z)[(\partial u_{j-1,k-1}/\partial z) + (\partial u_{j+1,k+1}/\partial z) - (\partial u_{j-1,k+1}/\partial z) - (\partial u_{j+1,k-1}/\partial z)] \quad , \qquad \text{(A-6)}$$

$\partial^3 u_{j,k}/\partial x^2 \partial z = (31/864\Delta x^2 \Delta z)(u_{j+2,k+2} - u_{j-2,k-2} + u_{j-2,k+2} - u_{j+2,k-2} + 2u_{j,k-2} - 2u_{j,k+2})$

$+ (44/27\Delta x^2 \Delta z)(u_{j+1,k+1} - u_{j-1,k-1} + u_{j-1,k+1} - u_{j+1,k-1} + 2u_{j,k-1} - 2u_{j,k+1})$

$-(1/144\Delta x^2)[(\partial u_{j-2,k-2}/\partial z)+(\partial u_{j+2,k+2}/\partial z)+(\partial u_{j-2,k+2}/\partial z)+(\partial u_{j+2,k-2}/\partial z)-2(\partial u_{j,k+2}/\partial z)-2(\partial u_{j,k-2}/\partial z)]$

$-(4/9\Delta x^2)[(\partial u_{j-1,k-1}/\partial z)+(\partial u_{j+1,k+1}/\partial z)+(\partial u_{j-1,k+1}/\partial z)+(\partial u_{j+1,k-1}/\partial z)-2(\partial u_{j,k+1}/\partial z)-2(\partial u_{j,k-1}/\partial z)]$

$-(1/144\Delta x\Delta z)[(\partial u_{j-2,k-2}/x) + (\partial u_{j+2,k+2}/\partial x) - (\partial u_{j-2,k+2}/\partial x) - (\partial u_{j+2,k-2}/\partial x)]$

$-(4/9\Delta x\Delta z)[(\partial u_{j-1,k-1}/\partial x) + (\partial u_{j+1,k+1}/\partial x) - (\partial u_{j-1,k+1}/\partial x) - (\partial u_{j+1,k-1}/\partial x)] \quad ,$ \hfill (A-7)

where Δx, Δz denote the space increment in the x- and z-directions, respectively.

Similarly, the corresponding computational formulae related to the particle-velocity v can be obtained simply by substituting u by v into (A-1)-(A-7).